Torque Ripple Reduction of Synchronous Reluctance Machine by Using Asymmetrical Barriers and Hybrid Magnetic Core

Chengcheng Liu, *Member, IEEE*, Kelin Wang, Shaopeng Wang, Youhua Wang, and Jianguo Zhu, *Senior Member, IEEE*

***Abstract*—As there is no need of permanent magnet (PM) material and only silicon steel sheet required on the rotor, synchronous reluctance machine (SynRM) can be used for many applications and draws a great research interest. For the SynRM, the torque ripple is a big issue and a great of work could been done on reducing it. In this paper, asymmetrical magnetic flux barriers in the SynRM rotor were studied comprehensively, including angle and width of each layer and each side of the magnetic barrier. The SynRMb with asymmetrical and parallel magnetic flux barrier was found as the best way to design SynRM based on the multi-objective design optimization method. Moreover, each parameter was studied to show the design rule of the asymmetrical magnetic flux barrier. As the average torque will be reduced with the asymmetrical barrier is used, the grain-oriented silicon steel is used on stator teeth of the SynRMb (SynRMbG) was proposed and studied. The analysis results show that the proposed new method can make the SynRM have better performance.**

***Index Terms*—Torque ripple reduction, synchronous reluctance machine, asymmetrical barriers, hybrid magnetic core.**

I. Introduction

In recent years, the cost of high-performance rare earth permanent magnet (PMs) increases considerably, and there is a trend to develop electrical machine without using high cost PMs, e.g. PM machine with ferrite magnet and synchronous reluctance machine (SynRMs) [1]. The main advantages of the SynRMs include the low cost, high robust and good performance if compared with induction machine. The drawbacks of SynRMs include the low power factor and high torque ripple. In the last two decades, many works have been done to improve power factor and reduce torque ripple of SynRM, where maximizing saliency ratio is the main target [2], [3]. In the design of SynRM, the rotor topology plays an important role, and it has been found that three flux barrier layers rotor design is the best way to maximize the saliency ratio and reduce the manufacture complexity.

For the torque ripple reduction in SynRMs, the following methods have been proposed and verified. The harmonic current injection method has been implemented into the field winding to mitigate the harmonic torque ripple [4]. The step-shaped gradient flux barrier has been developed in the rotor core for reducing the torque ripple [5], [6]. The asymmetrical pole of rotor has been considered as a feasible method for torque ripple reduction in both the SynRM and PM machine [7-8]. Moreover, it has been shown that the torque ripple depends on the coupling relationship between the rotor structure and input current. In addition, the torque ripple can be reduced by improving the control algorithm and structure design, e.g. the switching-table-based direct torque control (ST-DTC) [9] and response surface method (RSM) [10]. Besides, some multi-objective design optimization methods are proposed for improving the main performance of electrical machine[11] [12].

In this paper, the asymmetrical flux barrier rotor topologies in the SynRM have been studied comprehensively for achieving lower torque ripple. As the average torque will be reduced with the torque ripple reducing, the grain-oriented silicon sheets are enrolled on the stator teeth to release the flux saturation in the stator core. The analysis results based on the finite element method (FEM) show that the torque ripple of the SynRM can be reduced greatly and both the power factor and average torque of SynRM can be increased by using the hybrid magnetic core.

II. Topologies And Comparison Of SynRM With Different Asymmetrical Barrier Structure

Fig. 1 shows the main magnetic topology of the SynRM, it can be seen that this machine has 4 rotor poles and 24 stator slots with distributed winding configuration. As the flux barrier topology plays an important role on the parameters and performance of the SynRM, each flux barrier layer has their own individual angle and width, as shown in Fig. 2. For the

Manuscript received September 01, 2020; revised December 13, 2020; accepted January 13, 2021. date of publication March 25, 2021; date of current version March 18, 2021.

This work was supported in part by the National Natural Science Foundation of China under Project 52007047, in part by the National Natural Science Foundation of China under Project 51877065, and in part by Natural Science Foundation of Hebei Province under Project E2019202220. *(Corresponding author: Prof. Youhua Wang).*

Chengcheng Liu, Kelin Wang, Shaopeng Wang, and Youhua Wang are with State Key Laboratory of Reliability and Intelligence of Electrical Equipment, Hebei University of Technology and Key Laboratory of Electromagnetic Field and Electrical Apparatus Reliability of Hebei Province, Hebei University of Technology, Tianjin, 300130, China (2016020@hebut.edu.cn, 2972390950@qq.com, 522396000@qq.com, wangyi@hebut.edu.cn).

Jianguo Zhu is with school of electrical and information engineering, University of Sydney, NSW 2007, Australia, (jianguo.zhu@sydney.edu.au).

Digital Object Identifier 10.30941/CESTEMS.2021.00003

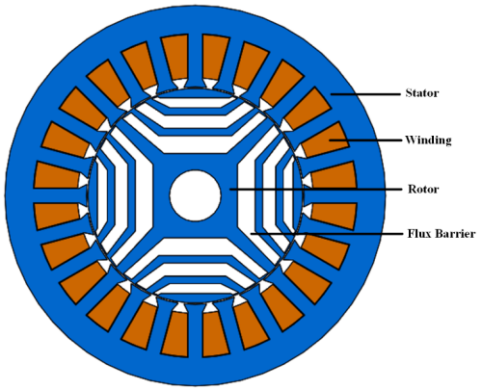

Fig. 1. Topology of SynRM.

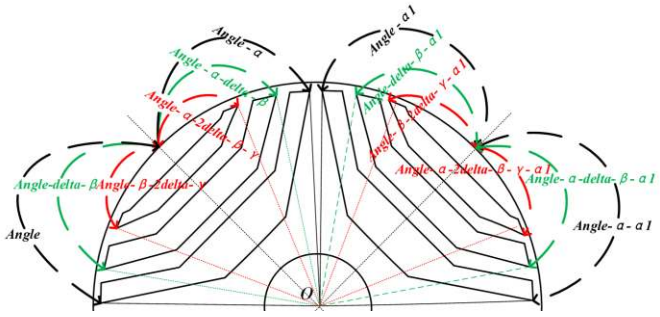

(a) Angle,

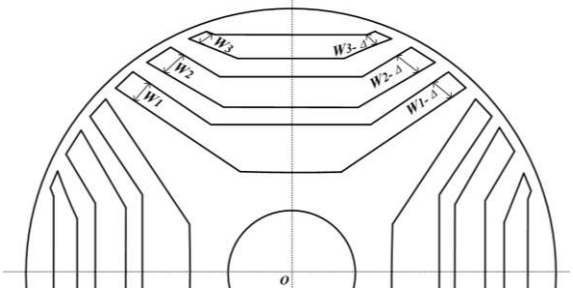

(b) Width.

Fig. 2. Parameters of flux barrier in SynRM rotor.

different pole pairs, they are symmetrical, while in one pole pair the adjacent rotor pole has a determined angle difference of α1, and for one rotor pole the adjacent side has a determined angle difference of α. For the different layers, the β and γ have been determined as angle difference between the first layer and second layer and the second layer and the third layer respectively. Between adjacent layers in one rotor pole, parameter Delta has been set to improve the relevance for three layers. As shown in Fig. 2(b), w1, w2 and w3 determine the width of flux barrier for each different layer, and the Δ determines the width difference for the different sides in one rotor pole.

For the final SynRM topology determination, the sequential design optimization method is used for the torque optimization of SynRM with different rotor topology configurations. Then four different topologies of SynRMs including the SynRMa with symmetrical and parallel magnetic flux barrier, SynRMb with asymmetrical and parallel magnetic flux barrier, SynRMc with symmetrical and non-parallel magnetic flux barrier, SynRMd with asymmetrical and non-parallel magnetic flux barrier are designed, optimized, and compared, as shown in Fig. 3. For each SynRM, the parameters e.g. the β, γ, Delta, are optimized.

The electromagnetic torque of SynRM can be calculated by

$$T = \frac{3}{4} p\left(L_d - L_q\right) i_s^{\,2} \sin(2\beta)$$

where p is number of pole pairs, i_s is the maximum value of the current in winding and β is the angle between the current and the d-axis.

Fig. 4 shows the main magnetic performance comparison among above SynRMs. Fig. 4(a) shows the electromagnetic

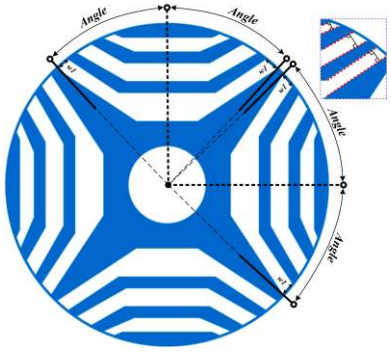

(a) Rotor for SynRMa

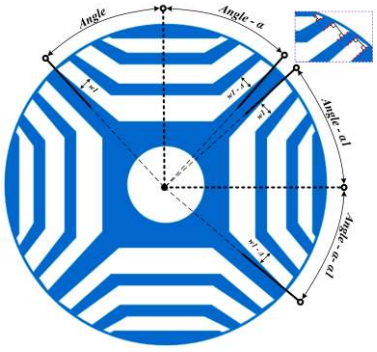

(b) Rotor for SynRMb

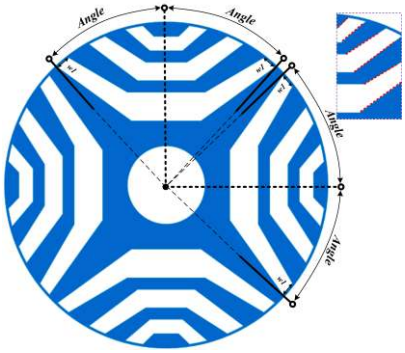

(c) Rotor for SynRMc

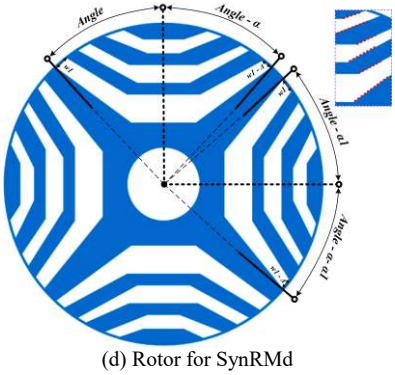

(d) Rotor for SynRMd

Fig. 3. Different rotor topologies

torque waveforms comparison versus the time with the maximum current density of 18 A/mm2. It can be seen that the average torque and torque ripple of SynRMa are 23.87 Nm and 3.66%, respectively, the average torque and torque ripple of SynRMb are 23.43 Nm and 1.57%, respectively, the average torque and torque ripple of SynRMc are 22.37 Nm and 13.39%, respectively, and the average torque and torque ripple of SynRMd are 23.33 Nm and 9.19%, respectively.

Through the comparison, it is seen that the SynRM with the parallel magnetic barrier design has higher electromagnetic torque, and in addition the SynRM with the asymmetrical magnetic barrier design has lower torque ripple. For the design optimization, the parameters defined in Fig. 2 are all considerate. Fig. 4(b) shows the multi objective design optimization of maximizing the average torque and minimizing the torque ripple of SynRMa and SynRMb, with the constraint of same stator design and maximum current density of 18 A/mm2. As shown, the SynRMb has much lower torque ripple but with only 1.7% average torque reduced. Therefore, for the SynRM design, the asymmetrical but parallel magnetic barrier is a good candidate. Fig. 4(c) shows the electromagnetic torque waveforms of the SynRMb along the clockwise direction and anticlockwise direction respectively. It can be seen that the average torque for the clockwise direction rotation is about 23.43 Nm while that for the anticlockwise direction rotation is about 23.62 Nm, which are pretty close. However, the torque ripple is 1.57% for the clockwise direction while that for the anticlockwise direction is about 7.63%. Therefore, the SynRMb can provide much lower torque ripple along the clockwise direction.

Fig. 5 shows the inductance comparison of four SynRMs.

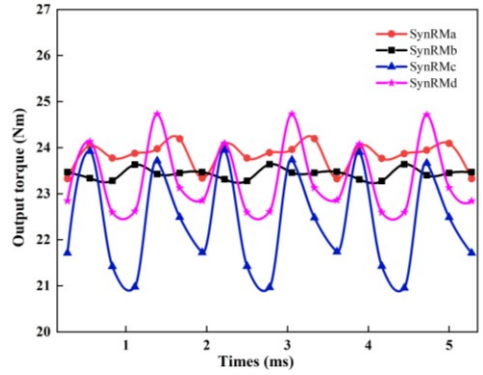

(a) Electromagnetic torque waveform of four SynRMs

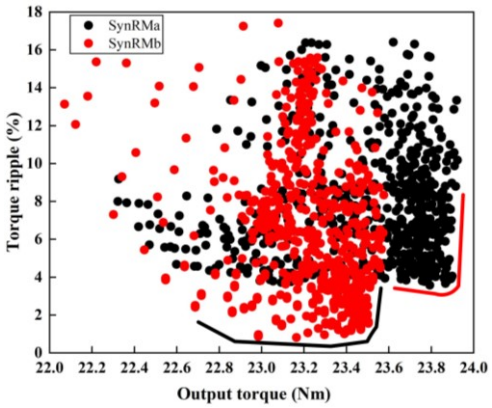

(b) Pareto front of SynRMa and SynRMb

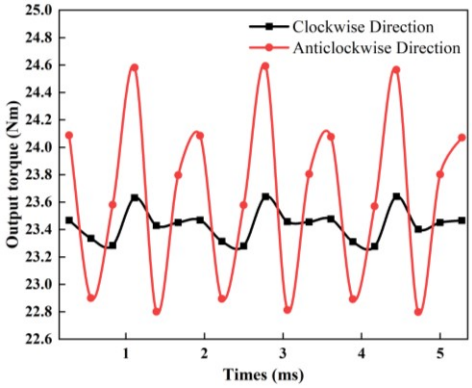

(c) Electromagnetic torque waveform of SynRM for different rotation direction

Fig. 4. Torque performance of four SynRMs with different rotor topologies.

The torque of SynRM is produced by the difference between the d axis inductance and q axis inductance. And the flux barrier is designed in SynRM, Ld is higher than Lq. As shown in Fig. 5(a), Ld of four SynRMs is very high when the input current density is low, however Ld will decrease rapidly firstly and decrease smoothly finally when the input current increase as Ld is influenced by magnetic saturation. While Lq of four SynRMs is quite stable as Lq is not influenced by saturation as the existence of flux barrier. Besides, the optimized result shows that Ld in SynRMc is the lowest, Ld in SynRMa and SynRMb is close and lower than that in SynRMd. The saliency ratio of these four SynRMs is shown in Fig. 5(b), in which the trend of Ld /Lq is same with Ld.

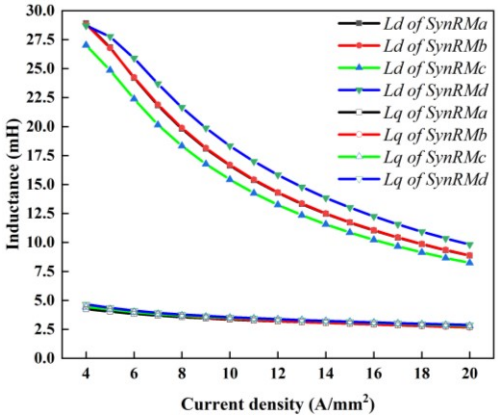

(a) Difference of L_d and L_q of four SynRMs

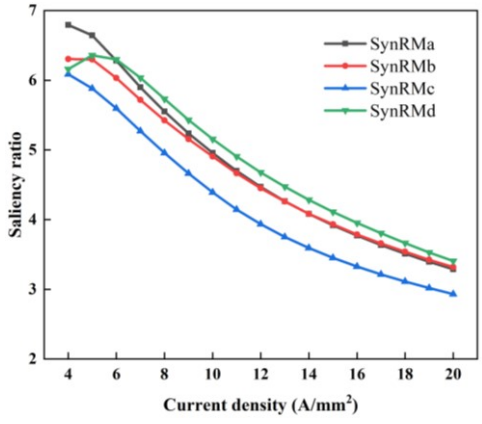

(b) Saliency ratio of four SynRMs

Fig. 5. Inductance performance of four SynRMs with different rotor topologies.

III. Parameter Analysis Of SynRM With Asymmetrical And Parallel Magnetic Flux Barrier

Fig. 6 shows the torque ripple of the SynRMb with the angle difference of the magnetic barrier between the adjacent rotor poles (α_1), the angle of the third magnetic barrier layer (Angle), and the angle difference between the different magnetic barrier layers (Delta), by using the FEM. It can be seen that the Angle and α_1 have the coupling effect on the torque ripple. When Angle is greater than 43.5 deg, the torque ripple of SynRMb will decrease with the α_1 increasing. However, when Angle is lower than 43.5 deg, then the torque ripple will increase with the α_1 increasing. And when Angle equals about 43.5 deg and α_1 equals about 1.5 deg, the torque ripple will achieve the minimum value of 1.46%. While for the Delta, it can be seen that when it equals about 9 deg, the torque ripple will achieve the minimum value. After the determination of the parameter of Delta, the other parameters of α, β and γ will be studied furtherly.

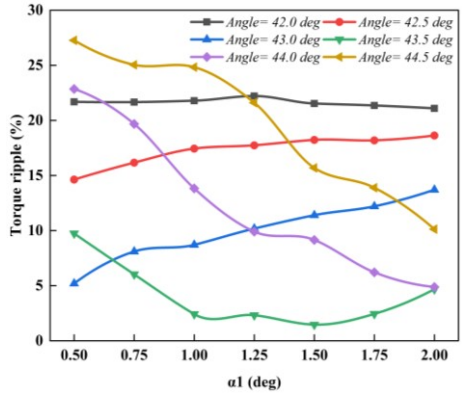

(a) Coupling effect of Angle and α_1

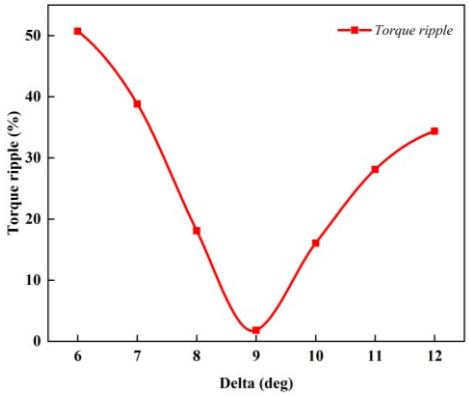

(b) effect of Delta

Fig. 6. Torque ripple of SynRMb with the variation of the parameters of Angle, α_1 and Delta.

Fig. 7, Fig. 8 and Fig. 9 show the torque ripple of SynRMb with the parameters of α, β and γ variation. After the comprehensively study, it can be seen that above parameters will have big effect on the torque ripple of the SynRM. Fig. 7(a) and Fig. 7(b) show that the torque ripple of SynRMb with the α and β variation from -1.25 deg to 1.25 deg and -1.0 deg to 1.0 deg, respectively. It can be seen that the torque ripple reaches the minimum value when β equals around -0.6 deg. When β equals around -0.6 deg, the torque ripple of SynRMb reaches the minimum value when α equals about 0.75 deg.

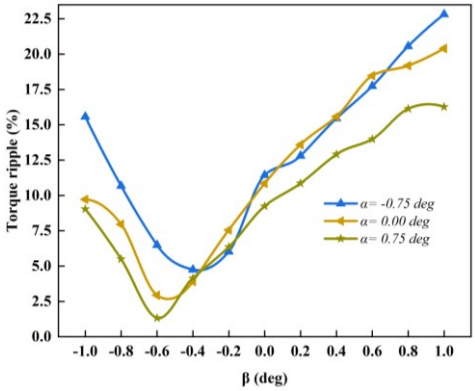

(a) Torque ripple optimizations of α and β

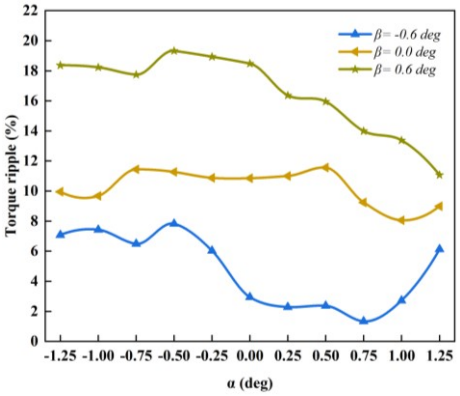

(b) Torque ripple optimizations of β and α

Fig. 7. Torque ripple optimizations for parameters of α, β and γ.

Fig. 8(a) and Fig. 8(b) shows the torque ripple of SynRMb with the α, and γ variation from -1.25 deg to 1.25 deg and -1.8 deg to 1.8 deg, respectively. It can be seen that when α equals about 0.75 deg, the SynRM will have minimum torque ripple. While for parameter γ, it can be seen that the torque ripple will decrease with the increase of γ, and the torque ripple of SynRM reaches its minimum when it is equal to about 1.8 deg.

Fig. 9(a) and Fig. 9(b) shows the torque ripple of SynRMb with the β and γ variation from -1.0 deg to 1.0 deg and -1.8 deg and 1.8 deg, respectively. As shown when β equals about -0.6 deg, the torque ripple will achieve minimum value, however it is difficult to make a determination of the parameter of γ, it can be seen that during the β variation, there is a trend for γ increasing, then the torque ripple decreases. However, if β equals about -0.6 deg, the minimum torque ripple can be achieved when γ equals about 1.0 deg.

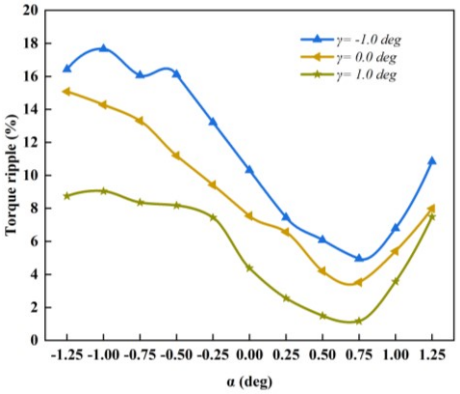

(a) Torque ripple optimizations of γ and α,

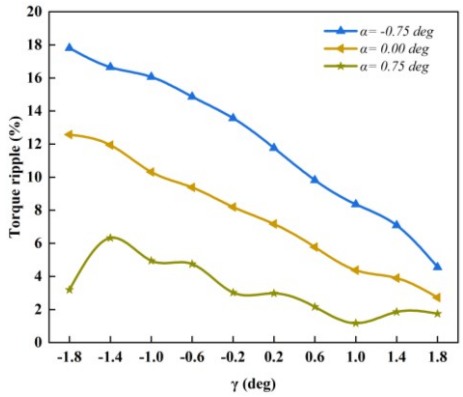

(b) Torque ripple optimizations of α and γ.

Fig. 8. Torque ripple optimizations for parameters of α and γ.

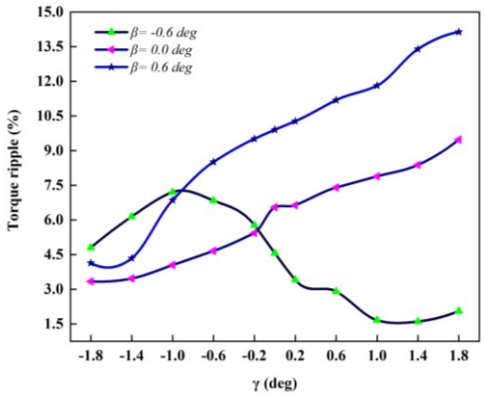

(a) Torque ripple optimizations of β and γ

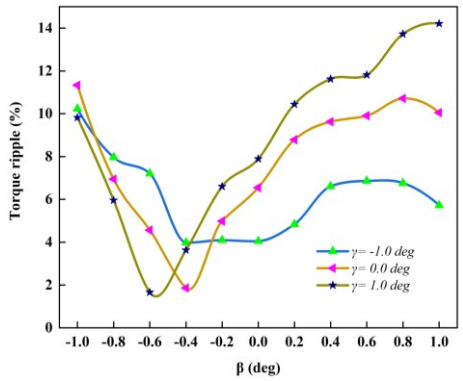

(b) Torque ripple optimizations of γ and β.

Fig. 9. Torque ripple optimizations for parameters of α, β and γ, (a), (b)

Besides the angle difference, the asymmetry of the width of magnetic barrier also plays an important role on the torque ripple of SynRM. Fig. 10 shows the torque ripple with the variation of Δ. It can be seen that when Δ equals about 0.1 mm, the minimum torque ripple can be achieved.

TABLE I
OPTIMIZED PARAMETER OF SYNRM WITH LOWEST TORQUE RIPPLE

Parameter	Optimal value
Angle (°)	43.5
α, β, γ (°)	0.75, -0.6, 1.8
α_1 (°)	1.25
w_1, w_2, w_3 (mm)	2.2, 2.5, 1.2
Δ (mm)	0.1

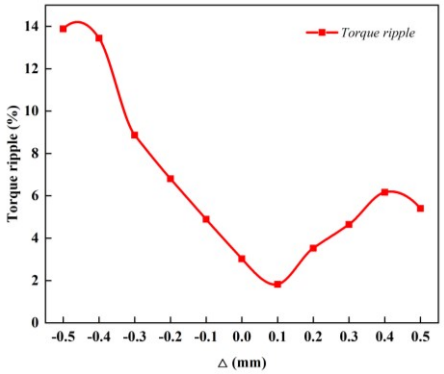

Fig. 10. The torque ripple optimization for parameter Δ.

By analyzing above parameters, it can be seen that the asymmetric design of the Angle and width of the magnetic barrier can greatly reduce the torque ripple of the SynRM, and Table I shows the final determination of the parameters of the SynRMb with the lowest torque ripple. For the first layer of magnetic flux barrier, the Angle is 43.5 deg and for another side the angle is about 42.75 deg which is determined by Angle -α=42.75°. For the second layer, the angle along the clockwise direction is 35.1 deg (Angle-Delta-β=35.1°), and for another side is 34.35 deg (Angle-α-Delta-β=34.35°). For the third magnetic flux barrier layer, the angle along the clockwise direction is 24.3 deg (Angle-2×Delta-β-γ=24.3°), and angle for another side is 23.55° (Angle-α-2×Delta-β-γ=23.55°). It can be seen that both the angle for the first, second and third magnetic flux barrier close to the clockwise direction need to be higher than that close to the anticlockwise direction. Moreover, for the angle difference of the adjacent layers between the first layer and second layer is higher than that between the second layer and third layer (Delta-β<Delta+γ). For the adjacent pole, the optimized parameter of α_1 is 1.25°. Besides the angle difference, it can be seen that the asymmetrical of the width of the magnetic flux barrier plays an important role as well.

IV. SYNCHRONOUS RELUCTANCE MACHINE WITH HYBRID MAGNETIC CORE

Based on above analysis, it can be seen that the asymmetrical design of the magnetic barrier in SynRM can make the torque ripple of the machine very low, however the average torque is decreased as well. For the performance improvement, the grain-oriented silicon steel sheets are proposed to replace some part of the stator teeth in this section, which is named as SynRMbG as shown in Fig. 11 and its main parameters are tabulated in Table II.

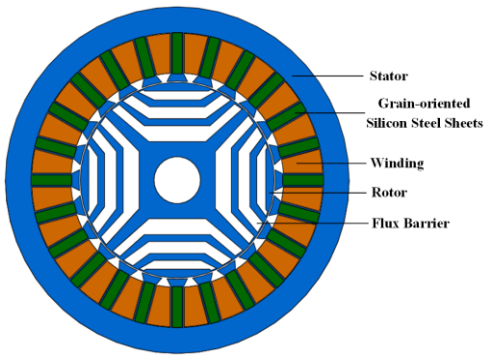

Fig. 11. Topology of SynRMbG.

By using FEM, the magnetic field distribution of the SynRM under the maximum current density of 18 A/mm^2 is calculated, as shown in Fig. 12. It can be seen that the magnetic flux density distributed on the grain-oriented silicon steel sheet on the stator teeth is much higher than other parts in the stator teeth. Fig. 12 shows the flux density comparison, it can be seen that the maximum magnetic flux density of SynRMbG can achieve 2.05T as the grain-oriented silicon steel sheet has very good performance along the rolling direction, while the maximum flux density of SynRMb is only 1.87 T.

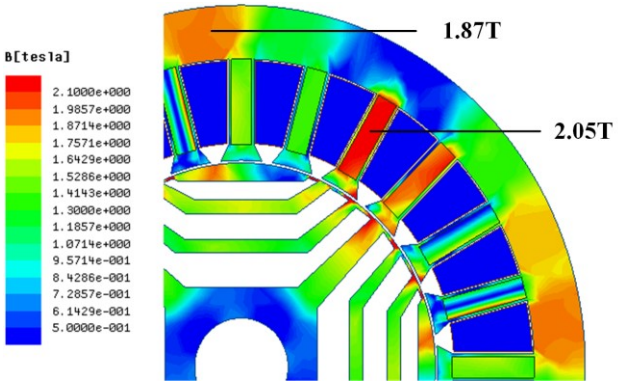

(a) Magnetic flux of SynRMbG

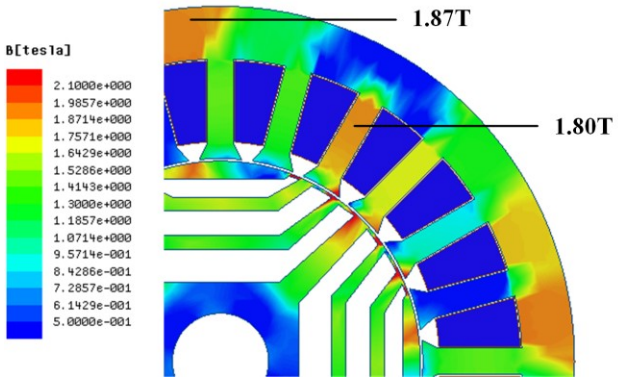

(b) Magnetic flux of SynRMb

Fig. 12. Electromagnetic analysis of magnetic flux.

Fig. 13 shows the main magnetic performance comparison among the SynRMaG (SynRMa with grain-oriented silicon steels), SynRMb and SynRMbG. It can be seen that the average torque of SynRMbG improves about 4.01% compared with SynRMb, however, the torque ripple increases from 1.57% to 2.38% as well. Although the average torque of SynRMaG is higher than others, the torque ripple is also higher obviously. Fig. 13(b) shows the efficiency and power factor comparison of SynRMaG, SynRMb and SynRMbG under the rated speed of 3000 rpm. As shown, the efficiency is improved about 0.4% during all the operation states as the torque is improved. Moreover, SynRMb and SynRMbG have little difference in power factor, however it can be seen that when the current density is higher than 10 A/mm^2, the power factor of the new machine is increased, as the saliency ratio of the SynRMb is increased. Besides, the power factor of SynRMaG is close to SynRMbG when the current density is higher than 7 A/mm^2.

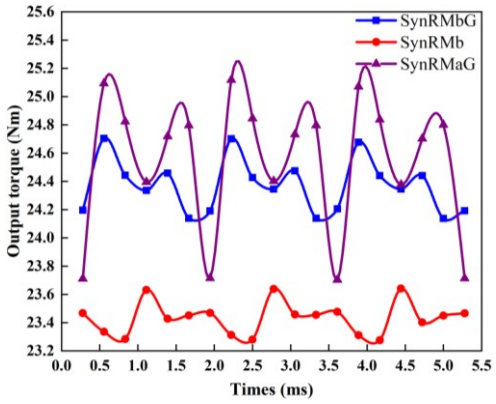

(a) Output Torque of SynRMb, SynRMaG and SynRMbG

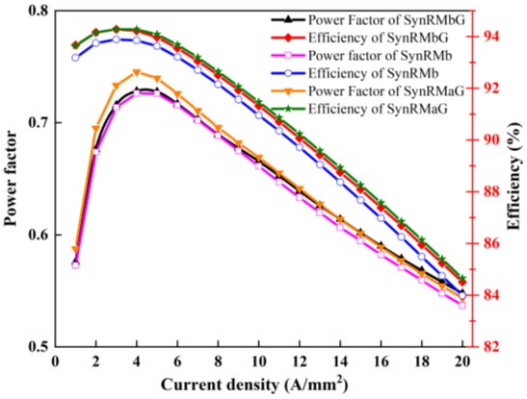

(b) Power Factor and Efficiency of SynRMb, SynRMaG and SynRMbG.

Fig. 13. SynRMs performance evaluation

Fig. 14(a) shows the calculated core loss of SymRM with different topologies under the rated speed of 3000 rpm, it can be seen that the core loss is reduced about 20% for the SynRMs of hybrid symmetric and asymmetric flux barriers. Fig. 14 (b) shows the efficiency comparison, it is seen that with the reduction of core loss, the efficiency can be improved. Fig. 15 shows the efficiency map of SynRMbG from the speed of 500 rpm to 6000 rpm, in which solid line represents the speed regulation curve of the max current density, and dotted line describes the speed regulation curve of the rated current density. In solid line, the efficiency of constant torque region can achieve 86%, and as well the efficiency of voltage region can reach 96%. Besides, in dotted line, the efficiency of constant torque region can achieve 92%, and as well the efficiency of voltage region can reach 96%.

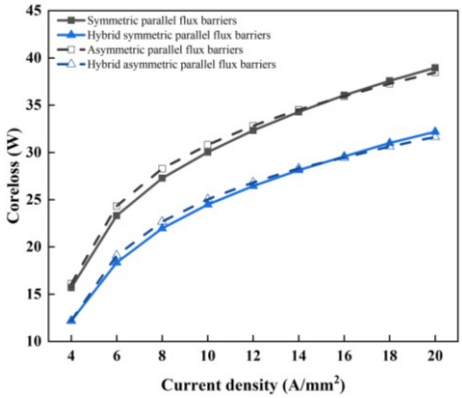

(a) Coreloss of SynRMs under the speed of 3000 rpm

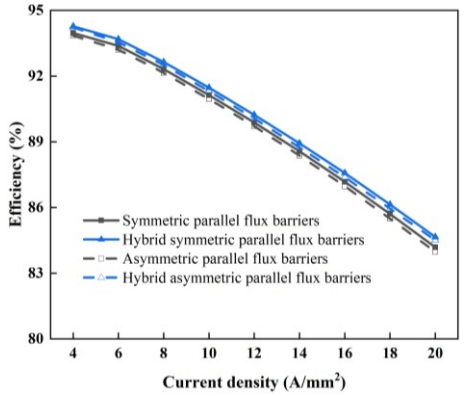

(b) Efficiency of SynRMs under the speed of 3000 rpm.

Fig. 14. SynRMs performance evaluation.

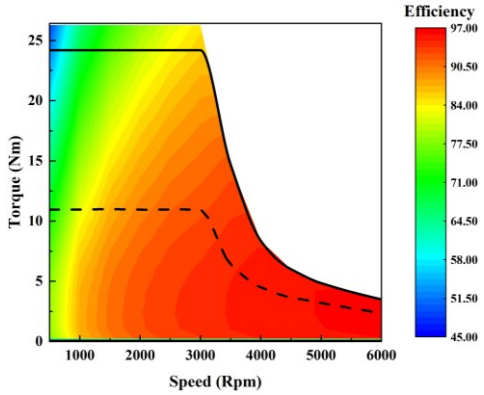

Fig. 15. Efficiency map of SynRMbG.

TABLE II
MAIN PARAMETERS OF SYNRMBG

Items	Proposed machine
Number of stator slot	24
Number of rotor pole	4
Stator outer/inner diameter	140/80
Rotor outer/inner diameter (mm)	79/19
Air gap length (mm)	0.5
Stack length (mm)	60
Rated speed (r/min)	3000
Rated current density (A/mm^2)	8
Max current density (A/mm^2)	18
Number of turns per slot	30

Mechanical stress analysis of the rotor was completed in Workbench. Using finite element software, the three-dimensional (3-D) rotor of SynRMbG is designed and can be matched with Workbench. The analysis of mechanical stress has been calculated in ANSYS workbench. Using the FEM, the three-dimensional (3-D) rotor of SynRMbG has been designed, then the topology can be matched with the workbench. After setting material, mesh, speed and other set of rotor, it can be seen the von mises stress and magnitude of displacement of rotor of SynRMbG in Fig. 16. Under the speed of 6000 rpm, the max von mises stress is 7.6177 Mpa on the flux barrier in Fig. 16(a), and the max displacement 1.4656 μm is also on flux barrier in Fig. 16(b), whose deformation is acceptable.

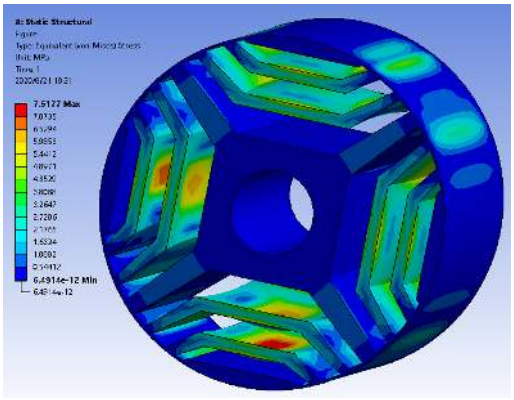

(a) Von mises stress of rotor for SynRM under the speed of 6000 rpm

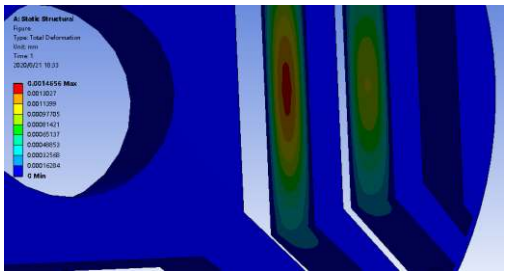

(b) Magnitude of displacement of rotor for SynRM under the speed of 6000 rpm.

Fig. 16. Von mises stress and magnitude of displacement of rotor for SynRM.

V. CONCLUSION

In this paper, the SynRM with the asymmetrical magnetic flux barrier was studied comprehensively. By using the multi-objective design optimization method, it was seen that SynRM with asymmetrical and parallel magnetic flux barrier had lower torque ripple, and both the asymmetrical of the angle and width work greatly. And the asymmetrical design principles of magnetic flux barriers are summarized as follows: the angle of magnetic flux barrier close to the clockwise direction needs to be higher than that close to the anticlockwise direction, the angle difference between the first layer and second layer is higher than that between the second layer and third layer, the symmetrical of the width of the magnetic flux barrier plays an important role as well. Moreover, for the performance improvement, the SynRMbG with the grain-oriented silicon steels replacing some part of the stator teeth were proposed, and it was seen that the average torque, efficiency and power factor were improved. For the SynRMbG, the analysis of temperature field and the design method of asymmetrical magnetic flux barrier in different power levels will be studied in the future work.

REFERENCES

[1] A. M. EL-Refaie et al., "Advanced High-Power-Density Interior Permanent Magnet Motor for Traction Applications," *IEEE Trans. Ind.* Appl., vol. 50, no. 5, pp. 3235-3248, September/October, 2014.

[2] W. Zhao, F. Xing, X. Wang, T. A. Lipo and B. Kwon, "Design and Analysis of a Novel PM-Assisted Synchronous Reluctance Machine With Axially Integrated Magnets by the Finite-Element Method," *IEEE Trans. Magn.*, vol. 53, no. 6, pp. 1-4, June, 2017.

[3] S. P. Wang, J.G. Ma, C. Liu, et al. "Design and performance analysis of a

novel synchronous reluctance machine," *IJAEM*, vol. 63, no. 2, pp. 249-265, Feb, 2020.

[4] B. Lee , Z. Q. Zhu, and L. Huang, "Investigation of Torque Production and Torque Ripple Reduction for Six-Stator/Seven-Rotor-Pole Variable Flux Reluctance Machines," *IEEE Trans. Ind. Appl.*, vol. 55, no. 3, pp. 2510-2518, May/June, 2019.

[5] Dong, Yan, et al., "Design and Analysis for Torque Ripple Reduction in Synchronous Reluctance Machine." *IEEE Trans. Magn*., vol. 54, no. 11, pp. 1-5, Nov. 2018.

[6] Okamoto, Yoshifumi, et al., "Improvement of Torque Characteristics for a Synchronous Reluctance Motor Using MMA-based Topology Optimization Method," *IEEE Trans. Magn.*, vol. 54, no. 3, pp. 99, March, 2018.

[7] Sanada M, Hiramoto K, Morimoto S et al., "Torque Ripple Improvement for Synchronous Reluctance Motor Using Asymmetric Flux Barrier Arrangement," *2003 38th IASC. IEEE,* 2003.

[8] Kim, Ki-Chan, "A Novel Method for Minimization of Cogging Torque and Torque Ripple for Interior Permanent Magnet Synchronous Motor," *IEEE Trans. Magn.*, vol. 50, no. 2, pp. 793-796, Feb. 2014.

[9] Y. Ren and Z. Q. Zhu, "Reduction of both harmonic Current and torque ripple for dual three-phase permanent-magnet synchronous machine Using Modified switching-table-based direct torque control," *IEEE Trans. Ind. Electron.*, vol. 62, no. 11, pp. 6671-6683, Nov. 2015.

[10] Jae-Kwang Lee, Dong-Hoon Jung, et al., "A Study on the Synchronous Reluctance Motor Design for High Torque by Using RSM," *IEEE Trans. Magn.*, vol. 54, no. 3, pp. 99, Feb. 2018.

[11] X. Sun, Z. Shi, G. Lei, Y. Guo, and J. Zhu, "Multi-objective design optimization of an IPMSM based on multilevel strategy," IEEE Trans. Ind. Electron., vol. 68, no. 1, pp. 139-148, Jan. 2021.

[12] K. Diao, X. Sun, G. Lei, Y. Guo, and J. Zhu, "Multiobjective system level optimization method for switched reluctance motor drive systems using finite element model," IEEE Trans. Ind. Electron., vol. 67, no. 12, pp. 10055-10064, Dec. 2020.

Chengcheng Liu (S'14 – M'16) was born in Jiangsu, China in 1988. He received the B.E. degree in automation engineering from Yangzhou University, Yangzhou, China, in 2010 and the Ph.D. degree in electrical engineering from Hebei University of Technology, Tianjin, China, in 2016. He was a joint Ph.D. student supported by Chinese scholarship council in the University of Technology, Sydney, Australia.

He is currently a Lecturer of Hebei University of Technology, Tianjin China. His research interests include the design, analysis, control and optimization of electromagnetic devices.

Kelin Wang was born in Shandong, China in 1995. He received the B.E. degree in Electrical Engineering and Automation from Ludong University, Yantai, China, in 2018, where he is currently working toward the M.E. degree.

His current research interests include design and optimization of electromagnetic devices.

Shaopeng Wang was born in Hebei, China, in 1993. He received the B.E. and M.E degree in Electrical Engineering from Hebei University of Technology, Tianjin, China, in 2016 and 2019, where he is currently working toward the Ph.D. degree.

His current research interests include design and optimization of electromagnetic devices.

Youhua Wang received the B.E. degree from Xian Jiaotong University, Xian, China, in 1987; the M.E. degree from the Hebei University of Technology, Tianjin, China, in 1990; and the Ph.D. from Fuzhou University, Fuzhou, China, in 1994, all in electrical apparatus.

He is currently a Professor at the College of Electrical Engineering. His currently research interests include measurement and modeling of properties of magnetic materials, numerical analysis of the electromagnetic field, and electromagnetic device design, analysis and optimization.

Jianguo Zhu (S'90 – M'96 – SM'03) received the B.E. degree from Jiangsu Institute of Technology, Zhenjiang, China, in 1982; the M.E. degree from the Shanghai University of Technology, Shanghai, China, in 1987; and the Ph.D. degree from the University of Technology, Sydney (UTS), NSW, Australia, in 1995, all in electrical engineering.

He is currently a Professor of Electrical Engineering and the Head at the School of electrical and information engineering, University of Sydney. His current research interests include electromagnetic, magnetic properties of materials, electrical machines, and drives, power electronics, and green energy systems.